

Supporting Information

SWIR Emissive RosIndolizine Dyes with Nanoencapsulation in Water Soluble Dendrimers

Satadru Chatterjee,^a William E. Meador,^a Cameron Smith,^a Indika Chandrasiri,^a Mohammad Farid Zia,^b Jay Nguyen,^b Austin Dorris,^a Alex Flynt,^b Davita L. Watkins,^a Nathan I. Hammer,^a and Jared H. Delcamp^{*,a}

^a *Department of Chemistry and Biochemistry, University of Mississippi, Coulter Hall, University, MS 38677, USA.*

^b *Department of Biological Sciences, University of Southern Mississippi, Hattiesburg, MS 39406, USA*

*email: delcamp@olemiss.edu

Table of contents**Page**

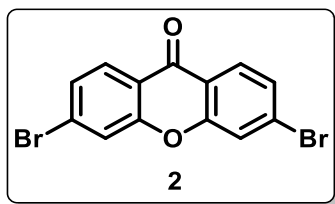
1. General Synthesis Information	S3
2. Synthetic Procedures	S4-S6
3. NMR Spectra	S7-S14
4. Synthesis Optimization, Nucleophile Scope and solubility data	S15-S16
5. Photophysical Spectroscopy	S17-S21
6. Computational Data	S22-S28
7. Nanoparticle Encapsulation	S29-S31
8. Cell Toxicity and Uptake	S32
9. References	S33

1. General Synthesis Information

All the reagents and solvents used in this study were purchased from Sigma Aldrich, Acros Organics and Thermo Fischer Scientific, respectively. The heating reactions were performed in an oil bath. All the ^1H and ^{13}C NMR spectra were recorded on a Bruker 400 MHz spectrometer using deuterated solvents. J values were expressed in Hz and chemical shifts were in ppm using tetramethylsilane (TMS) as a reference. Singlet (s), doublet (d), double doublet (dd) triplet (t) & multiplet (m) were designated as ^1H NMR multiplicity patterns. The mass analyzer was set to the 200–2000 Da range. Infrared spectra were recorded with an Agilent Cary 660 attenuated total reflection-Fourier transform infrared (ATR-FTIR). Fluorescence spectra were acquired using a Horiba QuantaMaster 8075–21 spectrofluorometer with xenon lamp excitation and liquid nitrogen cooled InGaAs solid-state detector. All the absorption profiles were recorded on a Cary 5000 UV-Vis-NIR spectrophotometer. Silica gel (230-400 mesh) were used for column chromatographic separations.

2. Synthetic Procedures

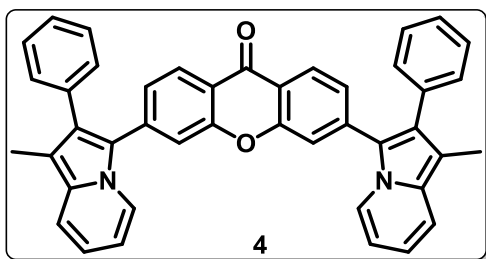
Synthesis of 3,6-dibromo-9H-xanthen-9-one (2):



To a solution of compound **1** (3.0 g, 6.7 mmol, 1.0 equiv.)¹ in 0.33 M MeOH:H₂O (1:1, 20 mL) under N₂, was added CuBr₂ (9.0 g, 40 mmol, 6.0 equiv.), and the reaction was heated to reflux overnight. The solid product was filtered and dissolved in DCM and washed with water and brine (30 mL x 3). The organic layer was then collected over Na₂SO₄, dried under reduced vacuum and purified using DCM/Hexane to get the desired product as a white solid in 83% (2.0 g, 5.6 mmol) yield.

¹H NMR (400 MHz, CDCl₃) δ 8.18 (d, J = 8.7 Hz, 2H), 7.69 (s, 2H), 7.54 (d, J = 8.6 Hz, 2H) ppm; ¹³C NMR (101 MHz, CDCl₃) δ 175.8, 156.0, 129.6, 128.1, 128.1, 121.1, 120.7 ppm; FTIR (ν_{max} , cm⁻¹): 3079, 2637, 2519, 2412, 2141, 2098, 2073, 1940, 1806, 1784, 1664, 1586, 1414, 1317, 1298, 1250, 1196, 1176, 1109, 1060, 937, 867, 838, 775, 706, 658; HRMS m/z calculated for C₁₃H₇Br₂O₂ [M+H]⁺ 352.8813, found 352.8680.

Synthesis of 3,6-bis(1-methyl-2-phenylindolizin-3-yl)-9H-xanthen-9-one (4):

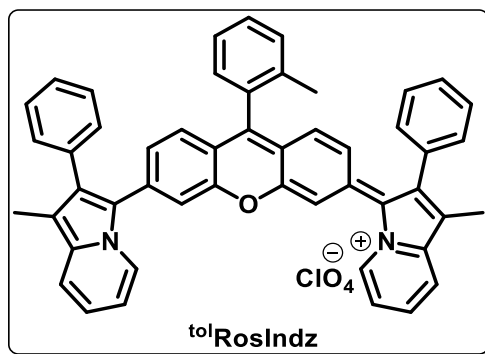


To a flame dried pressure flask in a glove box, was added compound **2** (300 mg, 0.85 mmol, 1.0 equiv.), 1-methyl-2-phenylindolizine (**3**) (351 mg, 1.69 mmol, 2 equiv.),² Pd(OAc)₂ (10 mg, 0.04 mmol, 0.05 equiv.), PCy₃*HBF₄ (31 mg, 0.08 mmol, 0.1 equiv.), Cs₂CO₃ (830 mg, 2.5 mmol, 3 equiv.), and dry toluene (0.04 M, 5 mL). The reaction was sealed and heated at 120°C for 72 hrs. The reaction mixture was filtered through a bed of Celite with DCM, washed with water then brine three times (30 mL). The organics were dried over Na₂SO₄, then the solvent was removed under reduced vacuum, and the product was purified by silica gel column chromatography using

acetone:hexane as eluent (1:3). The pure compound was isolated in 92% yield (473 mg, 0.77 mmol) as an orange solid.

^1H NMR (400 MHz, CDCl_3) δ 8.26 – 8.20 (m, 4H), 7.43 (d, J = 8.9 Hz, 2H), 7.39 (s, 2H), 7.35 – 7.28 (m, 6H), 7.25 – 7.18 (m, 6H), 6.76 (t, J = 6.5 Hz, 2H), 6.52 (t, J = 6.9 Hz, 2H), 2.35 (s, 6H) ppm. ^{13}C NMR (101 MHz, CDCl_3) δ 176.1, 156.5, 138.4, 134.9, 131.8, 130.7, 129.6, 128.3, 128.2, 126.9, 126.7, 125.8, 121.9, 120.3, 119.9, 117.9, 117.4, 111.3, 108.5, 9.2 ppm. FT-IR (ν_{max} , cm^{-1}): 3417, 3117, 3058, 2920, 2859, 1652, 1599, 1549, 1521. HRMS m/z calculated for $\text{C}_{43}\text{H}_{30}\text{N}_2\text{O}_2$ $[\text{M}]^+$ 606.2307, found 606.2318.

Synthesis of $^{\text{tol}}$ RosIndz

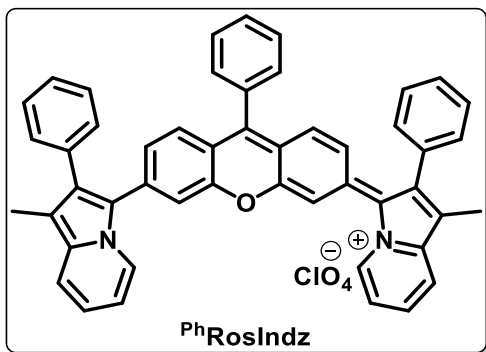


To a flame dried round bottom flask, was added compound **4** (50 mg, 0.08 mmol, 1 equiv.) and THF (0.02 M, 5 mL). The reaction was then sealed and cooled to -78°C . The solution was degassed with N_2 for 10 minutes, and then 5 equiv. of *o*-tolylmagnesium bromide (158 μL , 2.0 M in diethyl ether) was added to the mixture dropwise with constant stirring under N_2 . The reaction was stirred at room temperature and monitored via NMR until completion. Next, the THF was evaporated and the reaction mixture was diluted using DCM. A few drops of 2.0 M HClO_4 was added to the mixture, and the solution was shaken well in an extraction funnel until the formation of a dark green color occurred. The DCM layer was then washed with DI water to remove the excess acid and concentrated the organic layer under reduced vacuum. A large excess of diethyl ether was added to the oily solid mixture and the solids were separated by centrifuge to give the desired dye as a dark green solid (63%, 35 mg, 0.05 mmol). Note: this reaction has been performed on up to 300 mg scale with a similar yield obtained.

^1H NMR (400 MHz, CD_3CN) δ 8.71 (d, J = 7.0 Hz, 2H), 7.64 – 7.55 (m, 5H), 7.51 – 7.41 (m, 10H), 7.30 – 7.15 (m, 9H), 6.88 (t, J = 6.8 Hz, 2H), 2.24 (s, 6H), 2.04 (s, 3H) ppm. ^{13}C NMR (101 MHz, CD_3CN) δ 157.5, 143.5, 137.7, 136.9, 134.9, 134.8, 131.8, 131.5, 131.1, 131.1, 130.3, 129.6, 129.3, 129.2, 128.3, 126.8, 126.5, 124.9, 124.2, 122.7, 118.9, 114.8, 114.6, 113.8, 19.5, 8.9 ppm.

FTIR (ν_{max} , cm^{-1}): 3203, 3060, 3026, 2918, 2860, 2763, 2664, 2328, 1629, 1580, 1525, 1495, 1443, 1422, 1401, 1384, 1351, 1230, 1245, 1181, 1134, 1093, 1055, 1016, 982, 923, 893.; HRMS m/z calculated for $\text{C}_{50}\text{H}_{37}\text{N}_2\text{O}$ $[\text{M}]^+$ 681.2900, found 681.2926.

Synthesis of PhRosIndz



To a flame dried round bottom flask, was added compound **4** (40 mg, 0.06 mmol, 1.0 equiv.) and dry THF (0.02 M, 5 mL). The mixture was sealed and cooled to -78°C . The solution was degassed with N_2 for 10 minutes and then 5 equiv. of phenylmagnesium bromide (119 μL , 2.0 M in diethyl ether) was added to the mixture dropwise with constant stirring under N_2 . The reaction was left to stir at room temperature and monitored via NMR until completion. Then, the THF was evaporated, and the reaction mixture was diluted with DCM. A few drops of 2.0 M HClO_4 was added to the mixture, and the solution was shaken well in an extraction funnel until the formation of a dark green color occurred. The DCM layer was then washed with DI water to remove the excess acid and the organics were concentrated under reduced vacuum. A large excess of diethyl ether was then added to the oily solid mixture and the solids were separated by centrifuge to give the desired dye as a dark green solid (60%, 27 mg, 0.04 mmol).

^1H NMR (400 MHz, CD_3CN) δ 8.69 (d, $J = 7.0$ Hz, 2H), 7.72 – 7.67 (m, 3H), 7.62 (d, $J = 8.9$ Hz, 2H), 7.55 (s, 2H), 7.47 – 7.40 (m, 11H), 7.30 – 7.25 (m, 5H), 7.17 (t, $J = 6.6$ Hz, 2H), 6.87 (t, $J = 6.8$ Hz, 2H), 2.23 (s, 6H). ^{13}C NMR (101 MHz, CD_3CN) δ 157.5, 143.3, 137.7, 134.9, 134.7, 131.5, 131.1, 130.8, 130.3, 129.6, 129.3, 129.0, 128.5, 128.3, 124.9, 124.1, 122.6, 118.9, 114.8, 114.6, 113.8, 8.9; FTIR (ν_{max} , cm^{-1}): 3621, 3512, 3434, 3206, 3058, 2919, 2859, 2773, 2665, 2619, 2502, 2410, 2384, 2335, 2006, 1911, 1627, 1576, 1522, 1493, 1444, 1420, 1401, 1384, 1347, 1297, 1243, 1178, 1133, 1090, 1054, 1017, 984, 889; HRMS m/z calculated for $\text{C}_{49}\text{H}_{35}\text{N}_2\text{O}$ $[\text{M}]^+$ 667.2744, found 667.2758.

3. NMR Spectra

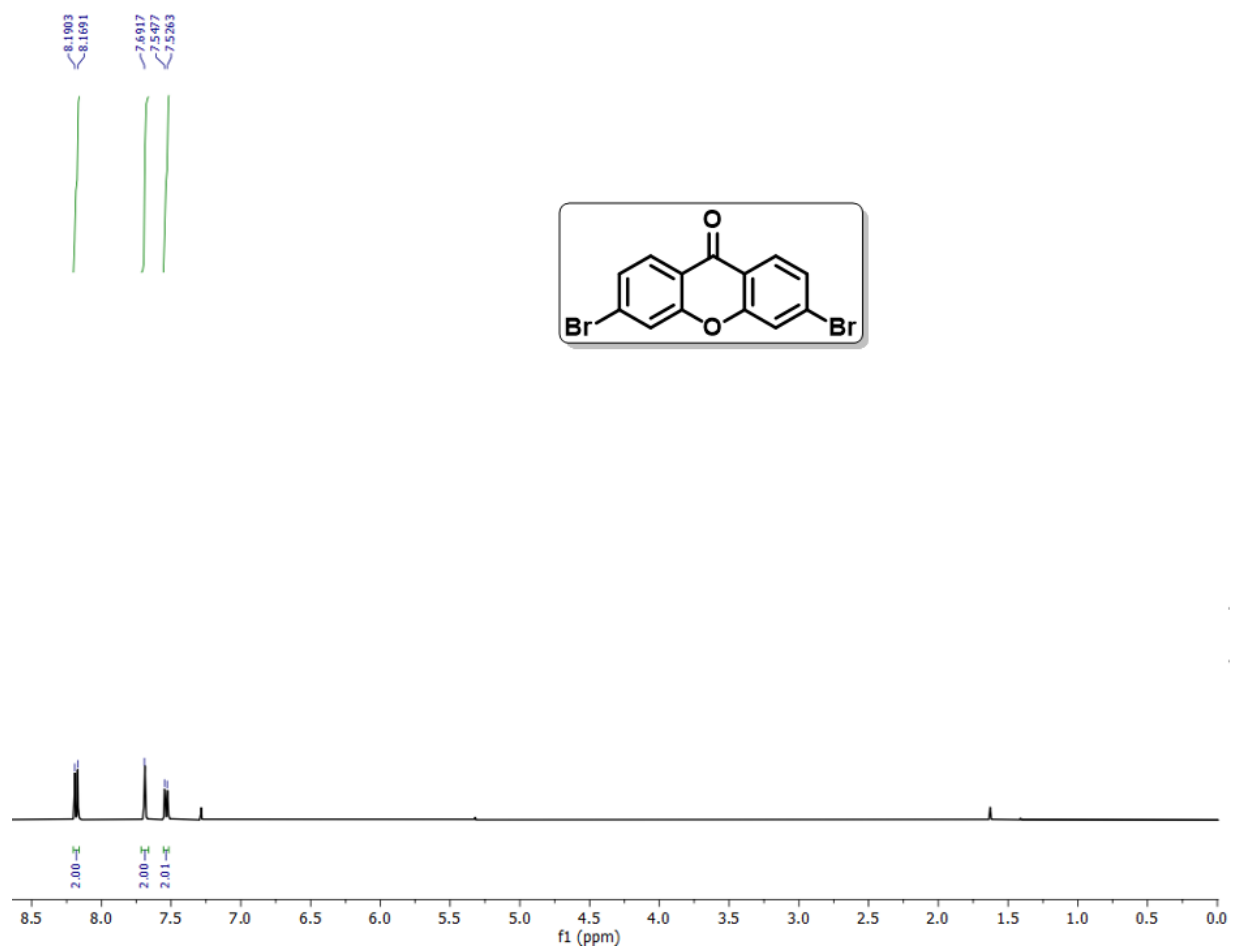


Figure S1. ^1H NMR (400 MHz) of compound **2** in CDCl_3 . The signal near 1.5 ppm is H_2O . The signal near 7.25 ppm is CHCl_3 .

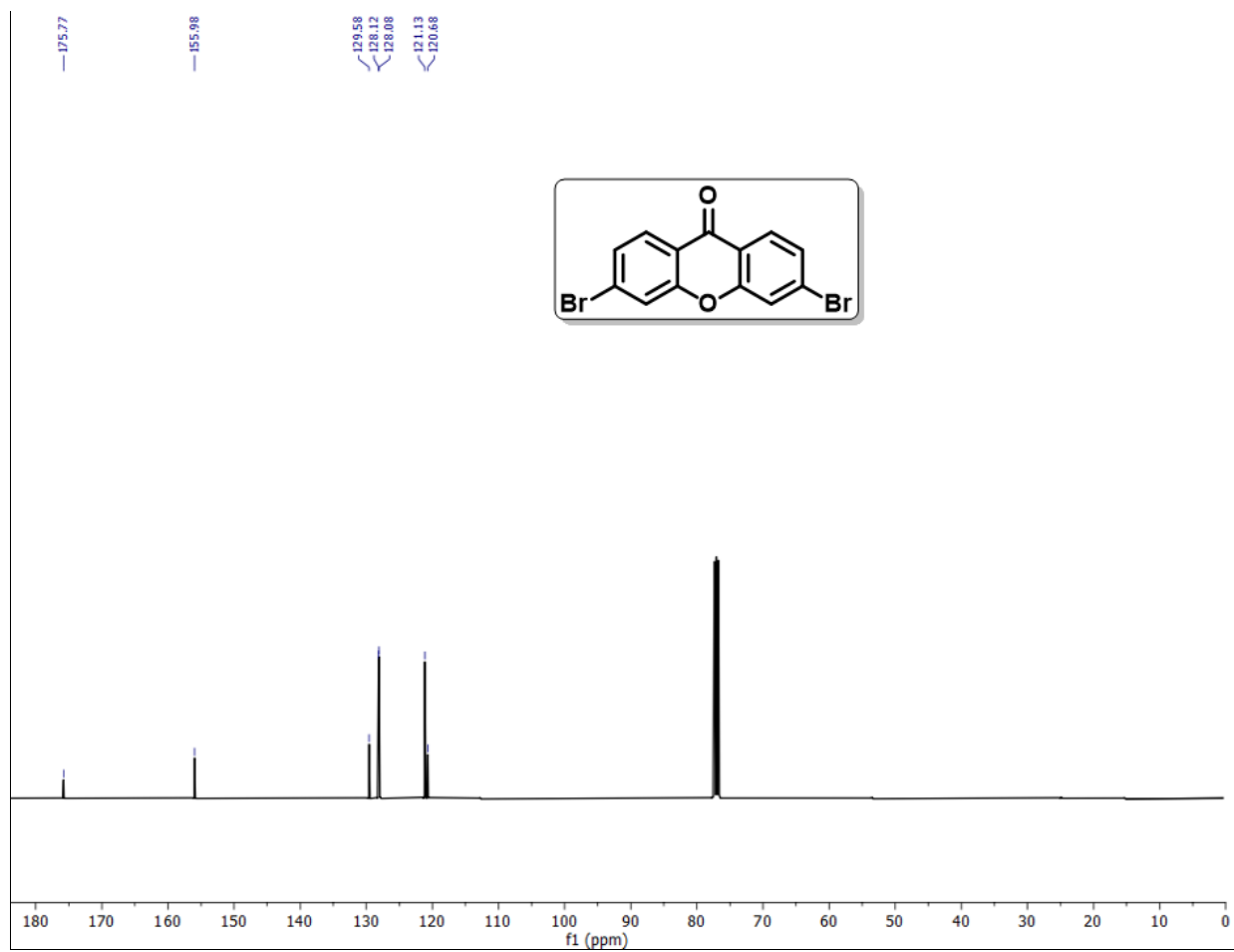


Figure S2. ^{13}C NMR (101 MHz) of compound **2** in CDCl_3 .

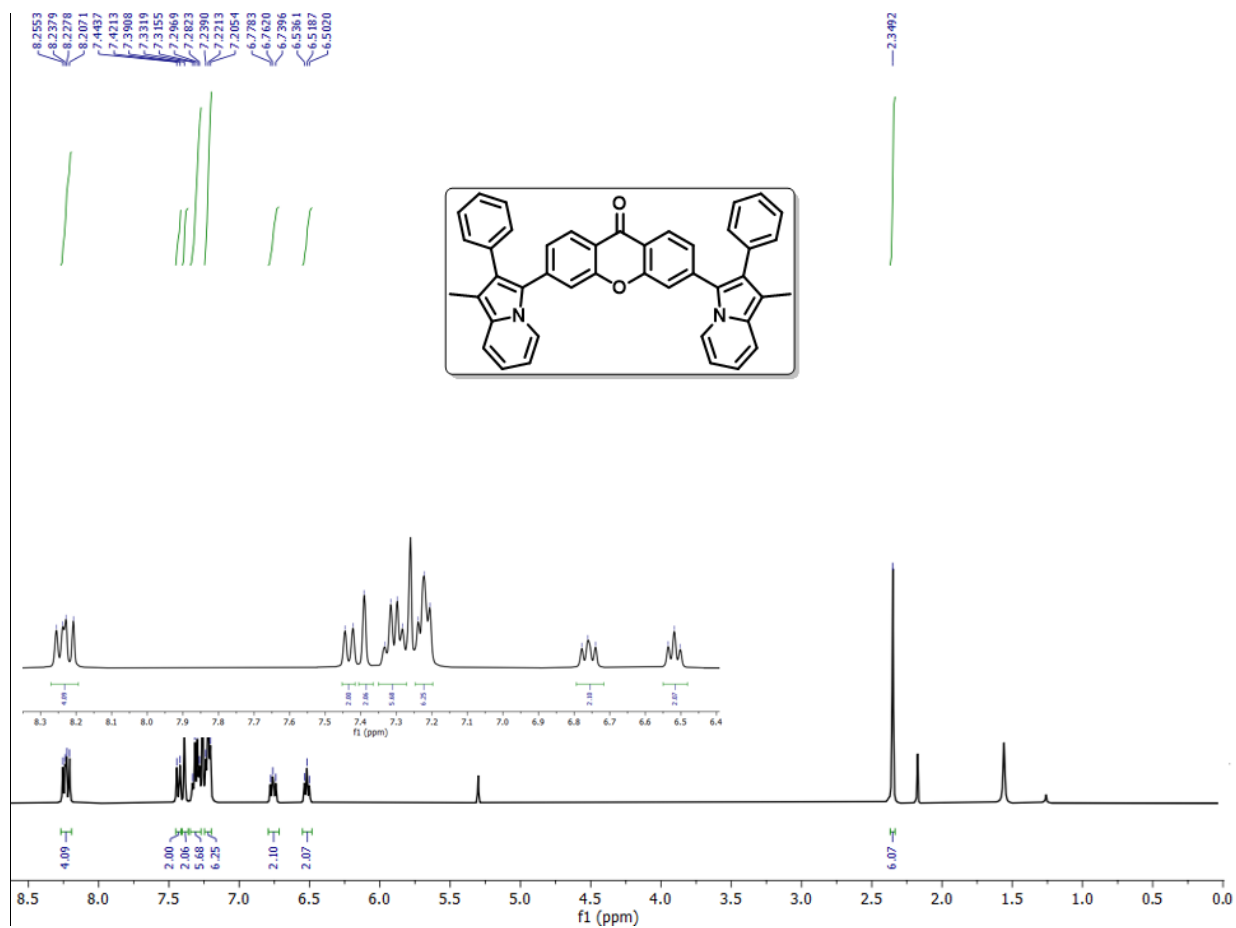


Figure S3. ¹H NMR (400 MHz) of compound 4 in CDCl₃. The signal near 7.25 ppm is CHCl₃. The signal near 5.25 ppm is dichloromethane. The signal near 2.1 ppm is acetone. The signal near 1.5 ppm is H₂O.

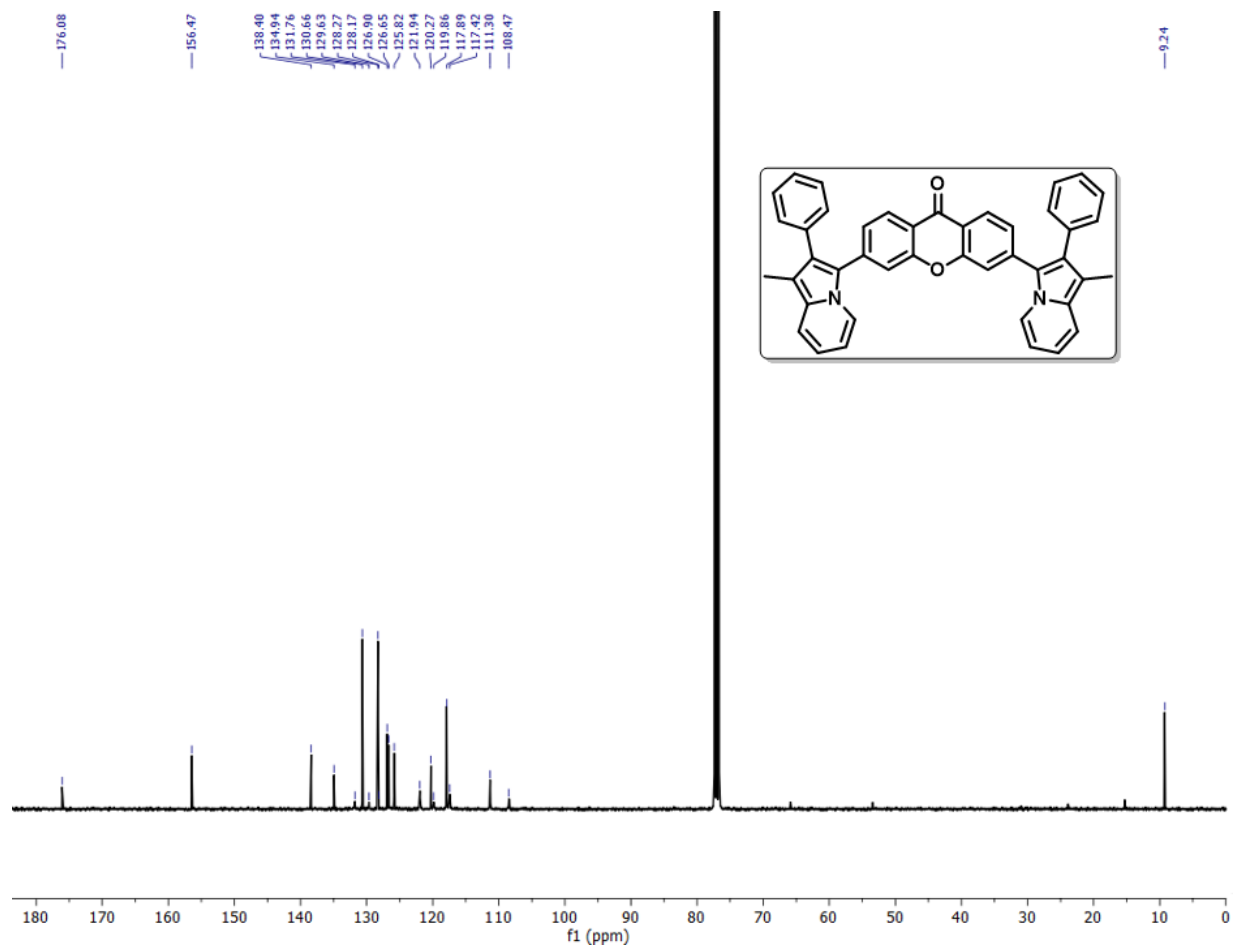


Figure S4. ^{13}C NMR (101 MHz) of compound **4** in CDCl_3 .

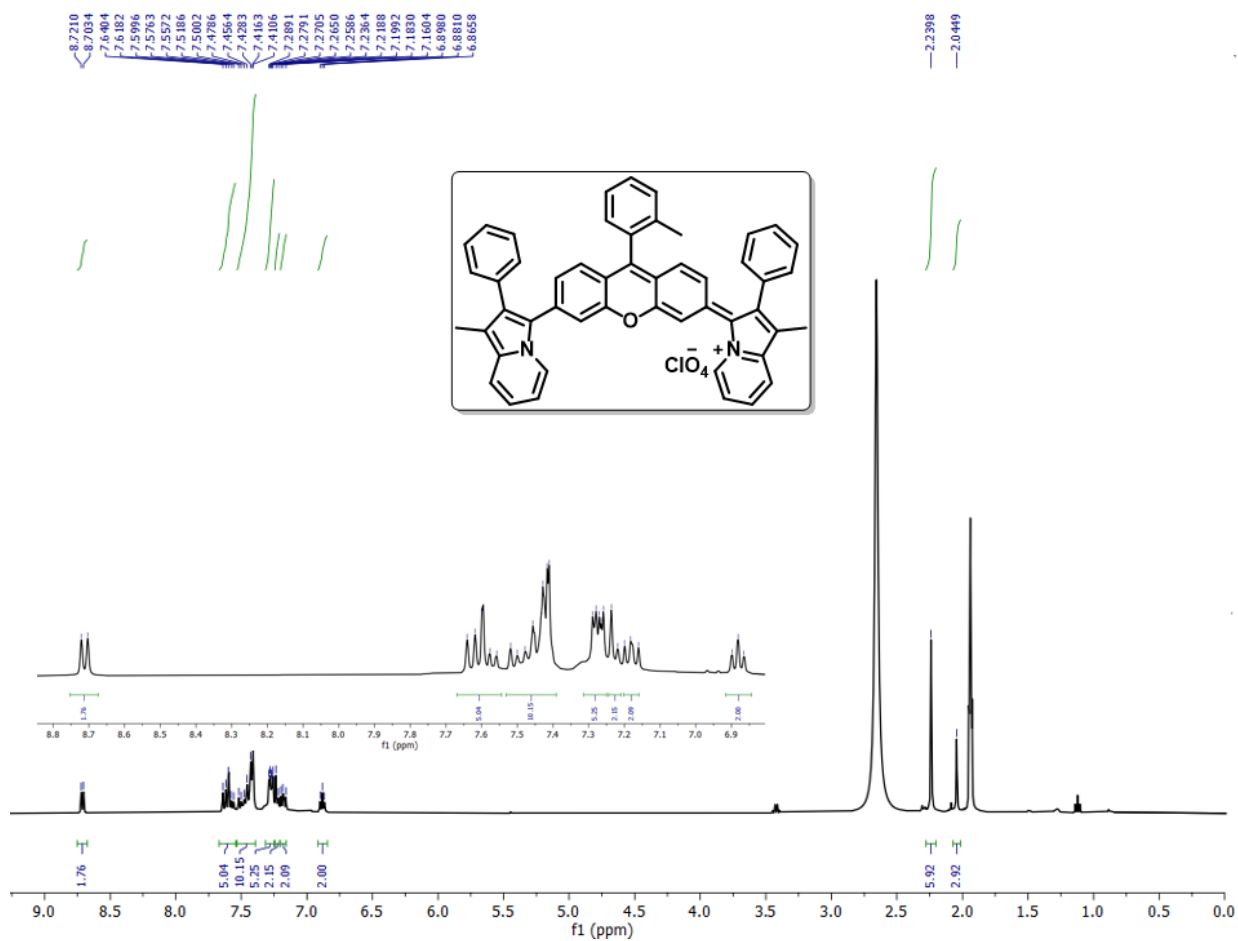


Figure S5. ^1H NMR (400 MHz) of $^{10}\text{lRosIndz}$ in CD_3CN . The signals near 3.5 and 1.0 ppm are diethyl ether. The signal near 2.5 ppm is H_2O . The signal near 2.0 ppm is residual acetonitrile solvent.

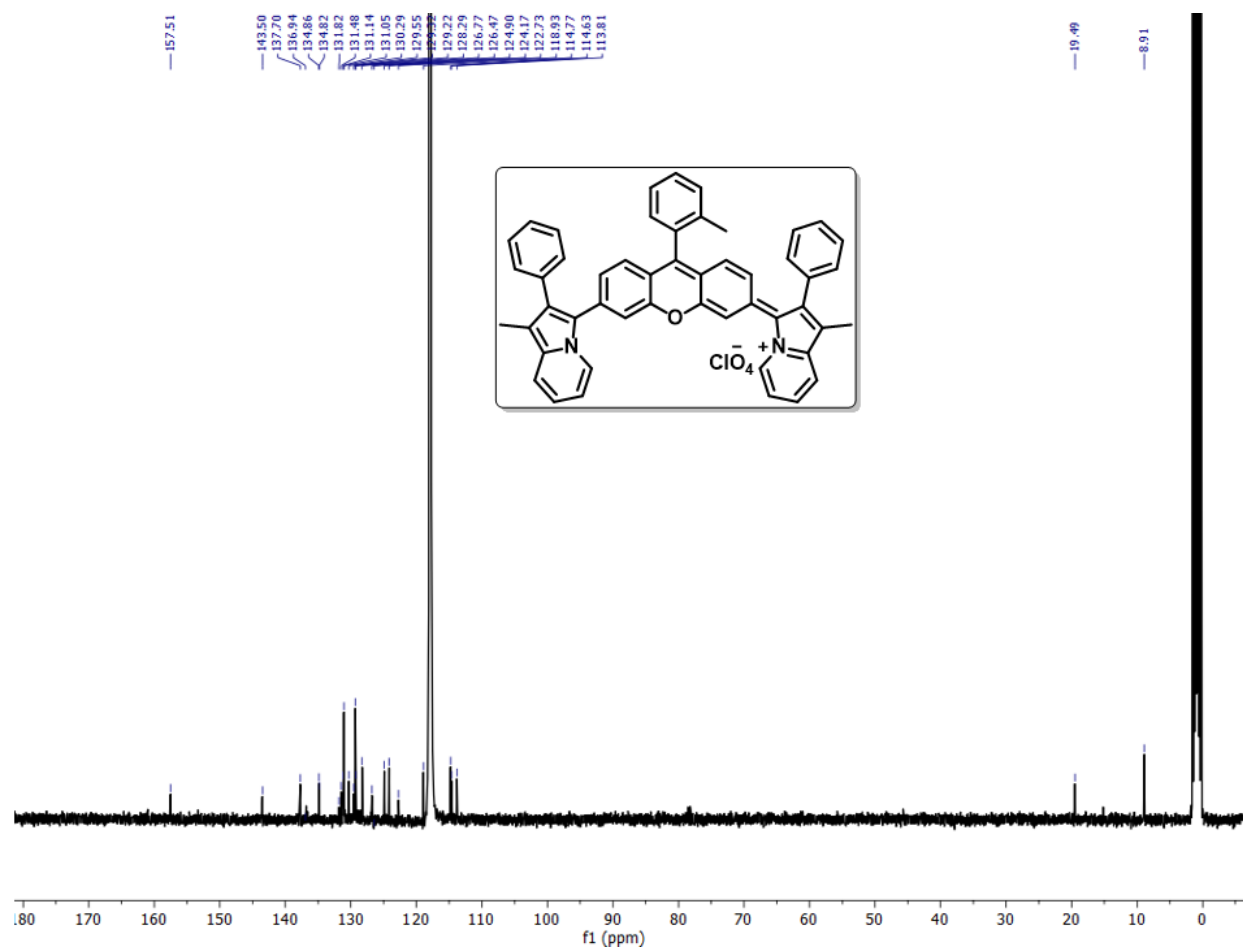


Figure S6. ^{13}C NMR (101 MHz) of $^{\text{tol}}\text{RosIndz}$ in CD_3CN .

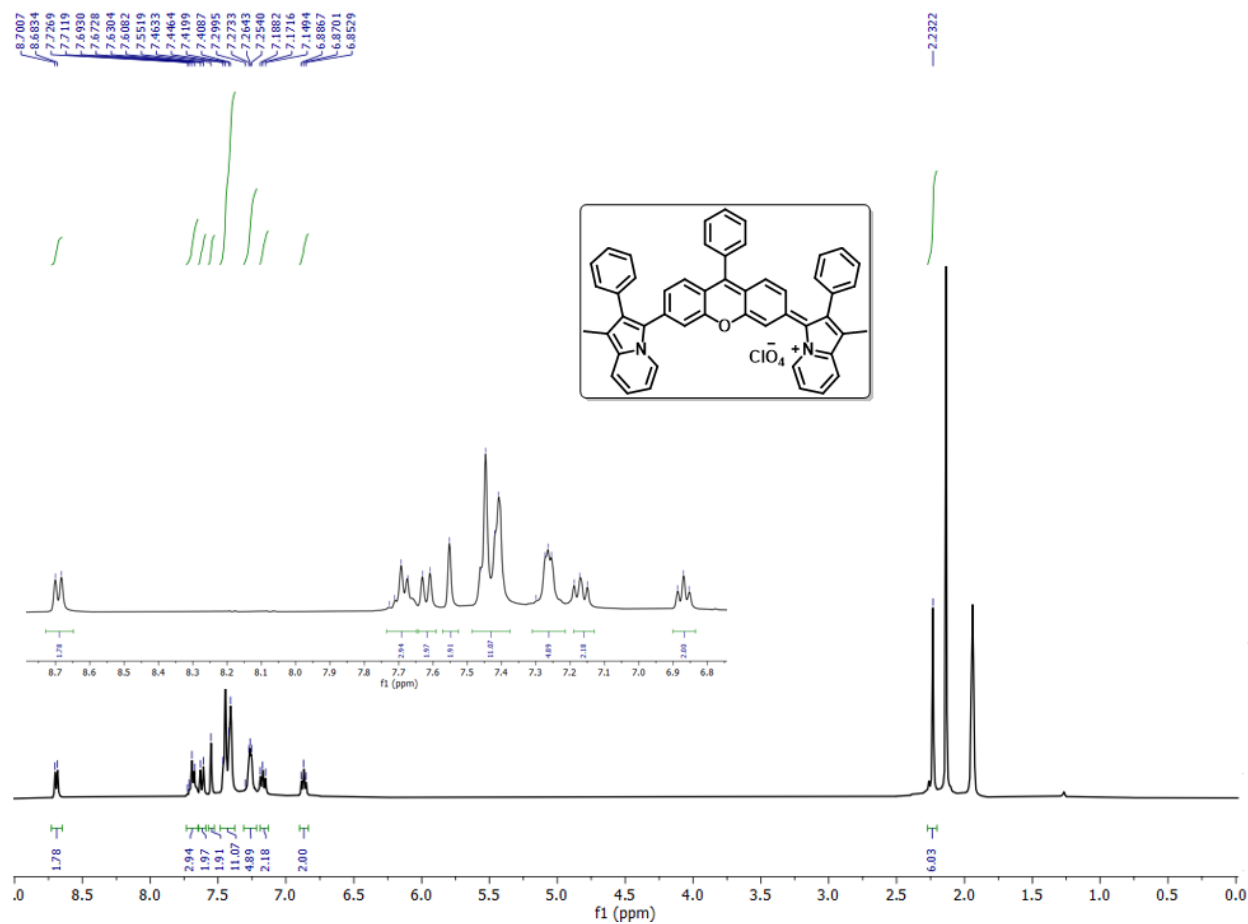


Figure S7. ^1H NMR (400 MHz) of PhRosIndz in CD_3CN . The signal near 2.2 ppm is H_2O . The signal near 2.0 ppm is residual acetonitrile solvent.

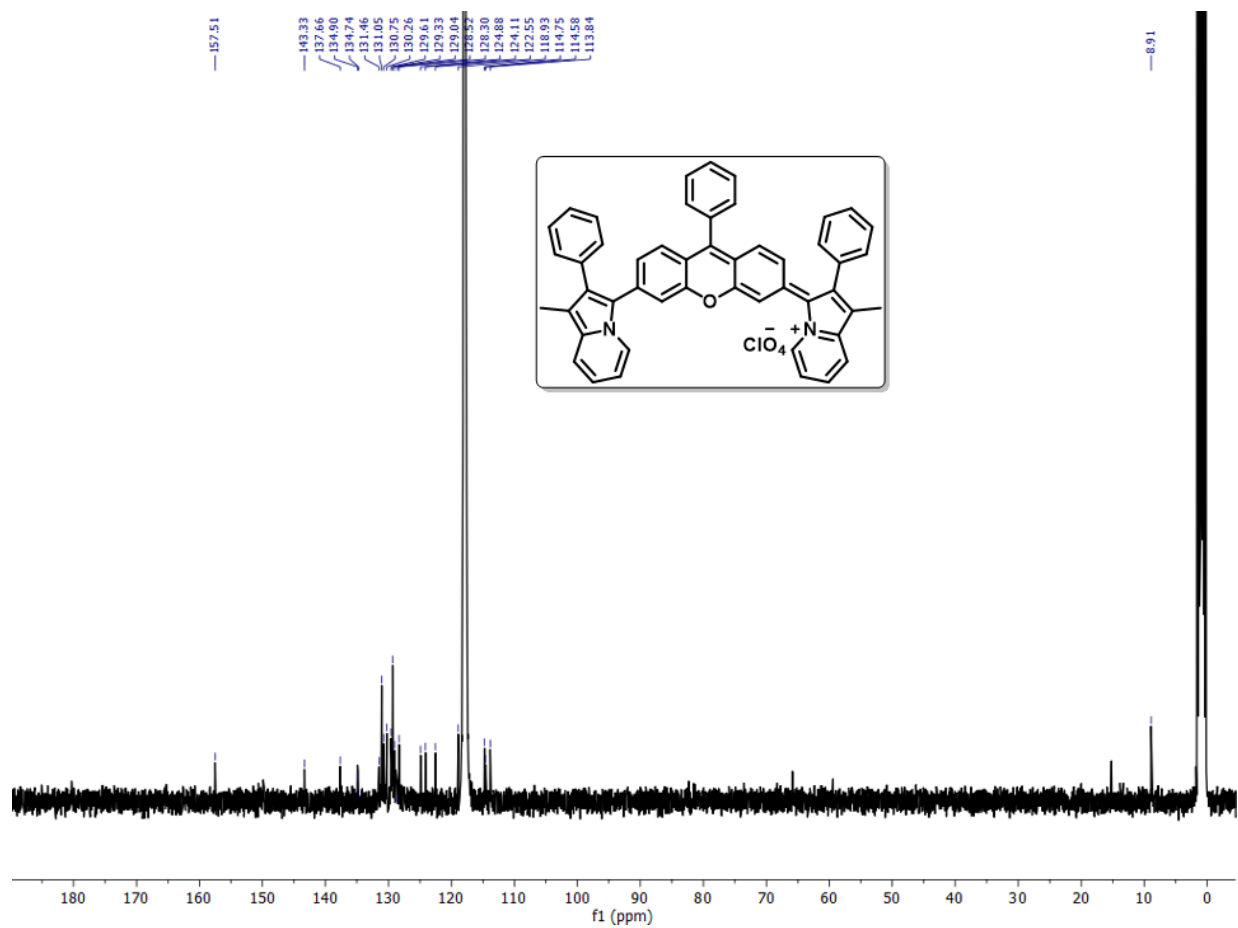


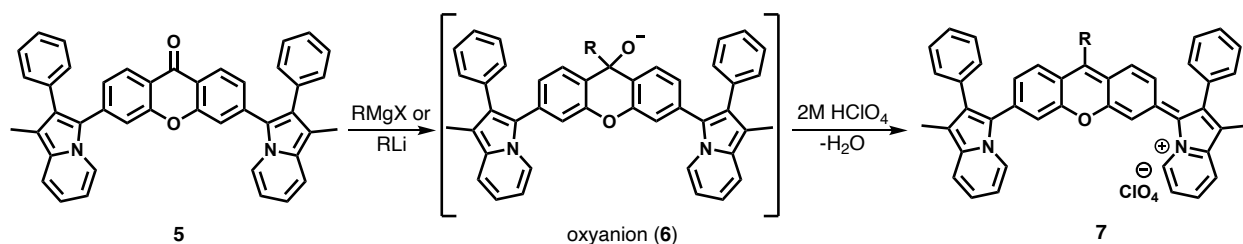
Figure S8. ^{13}C NMR (101 MHz) of $^{\text{Ph}}\text{RosIndz}$ in CD_3CN .

4. Synthesis Optimization and Nucleophile Scope Tables

Table S1: Optimization of the C-H activation reaction conditions.

Entry	Catalyst (5 mol%)	Ligand (10 mol%)	Base (3 eq.)	Solvent	Temp.	Yield
1	PdCl ₂ (PPh ₃) ₂	-	KOAc	Toluene	100°C	42%
2	PdCl ₂ (PPh ₃) ₂	-	Cs ₂ CO ₃	Toluene	100°C	17%
3	PdCl ₂ (PPh ₃) ₂	-	K ₃ PO ₄	Toluene	100°C	31%
4	PdCl ₂	Xphos	K ₃ PO ₄	Toluene	100°C	9%
5	Pd(OAc) ₂	XPhos	Cs ₂ CO ₃	Toluene	100°C	12%
6	Pd(OAc) ₂	P ^t Bu ₂ Me.HBF ₄	Cs ₂ CO ₃	Toluene	100°C	45%
7	Pd(OAc) ₂	PCy ₃ .HBF ₄	Cs ₂ CO ₃	Toluene	100°C	64%
8	Pd(OAc) ₂	P(^t Bu) ₃ .HBF ₄	Cs ₂ CO ₃	Toluene	100°C	13%
9	Pd(OAc) ₂	PCy ₃ .HBF ₄	Cs ₂ CO ₃	NMP	100°C	59%
10	Pd(OAc) ₂	PCy ₃ .HBF ₄	Cs ₂ CO ₃	Toluene	120°C	78%
11	Pd(OAc) ₂	PCy ₃ .HBF ₄	Cs ₂ CO ₃	Toluene	120°C	92% ^a

^aReaction ran for 72 hours. All other reactions were ran for 40 hours.



Scheme S1. Oxyanion formation and oxygen atom elimination with strong acid.

Table S2. Variety of nucleophiles used and the fate of the final product.

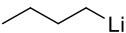
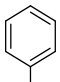
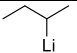
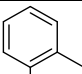
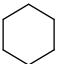
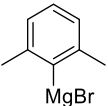
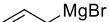
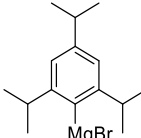
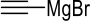
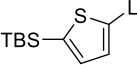
Entry	Nucleophile	Product	Entry	Nucleophile	Product
1	R= 	Formed and decomposed	6	 MgBr	Formed and isolated
2	 Li	Formed and decomposed	7	 MgBr	Formed and isolated
3	 MgCl	Formed and decomposed	8	 MgBr	Did not form
4	 MgBr	Did not form	9	 MgBr	Did not form
5	 MgBr	Did not form	10	 Li	Formed and decomposed

Table S3. Solubility of ^{tol}RosIndz in different solvents

Solvents	Solubility (mg/ml)
DCM	2
ACN	1.7
Toluene	0.3
THF	0.4

5. Photophysical Spectroscopy

Equipment and Experiment Details (Absorption)

Stability studies were performed by recording timepoint absorption maxima values of the dyes with a Cary 5000 UV-Vis-NIR spectrophotometer.

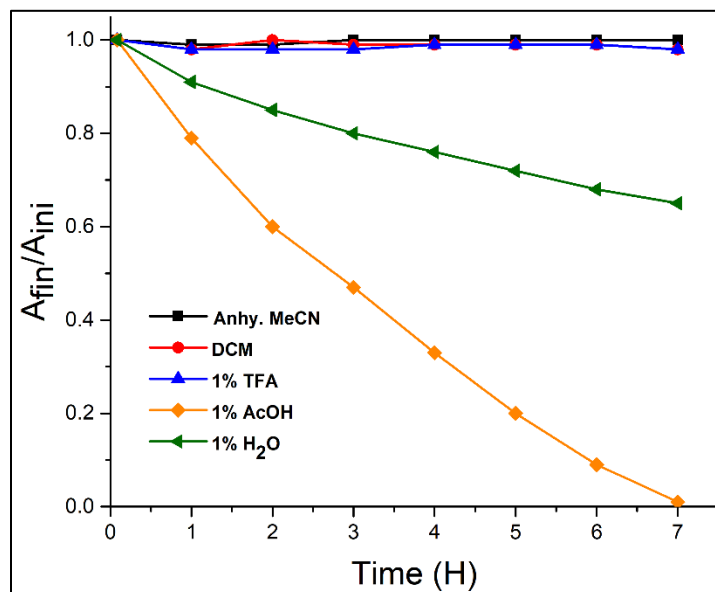


Figure S9. Stability studies of ^{tol}RosIndz under varying conditions in 99% MeCN unless otherwise specified.

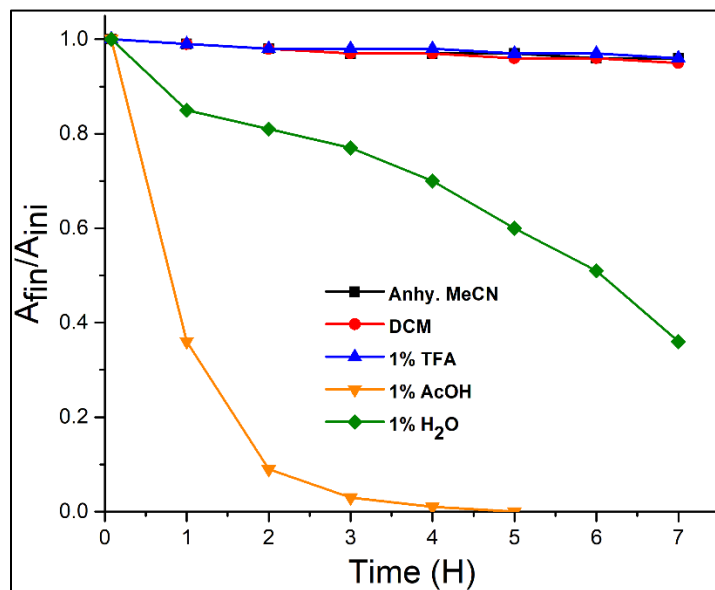


Figure S10: Stability studies of ^{Ph}RosIndz under varying conditions.

Equipment and Experiment Details (Emission)

The emission data was measured using a xenon-lamp based Horiba QuantaMaster spectrofluorometer under liquid N₂ cooled InGaAs detector. The excitation wavelength was 950 nm, and emission was measured from 975 to 1400 nm for both the free and encapsulated samples.

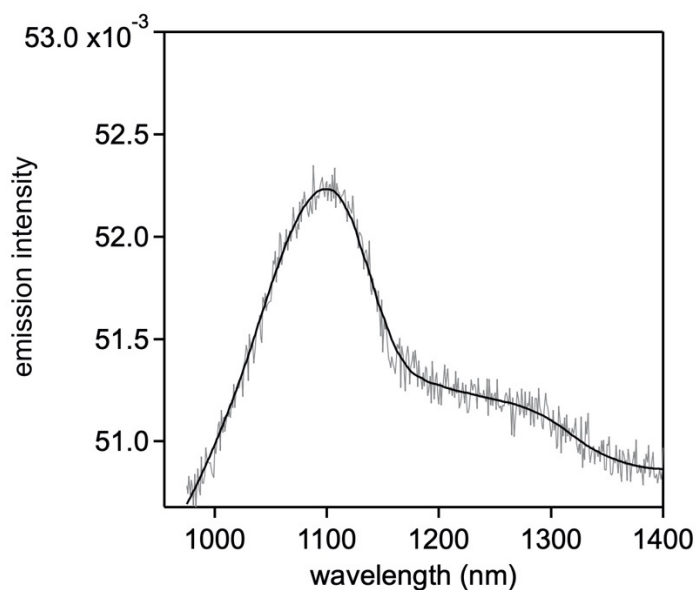
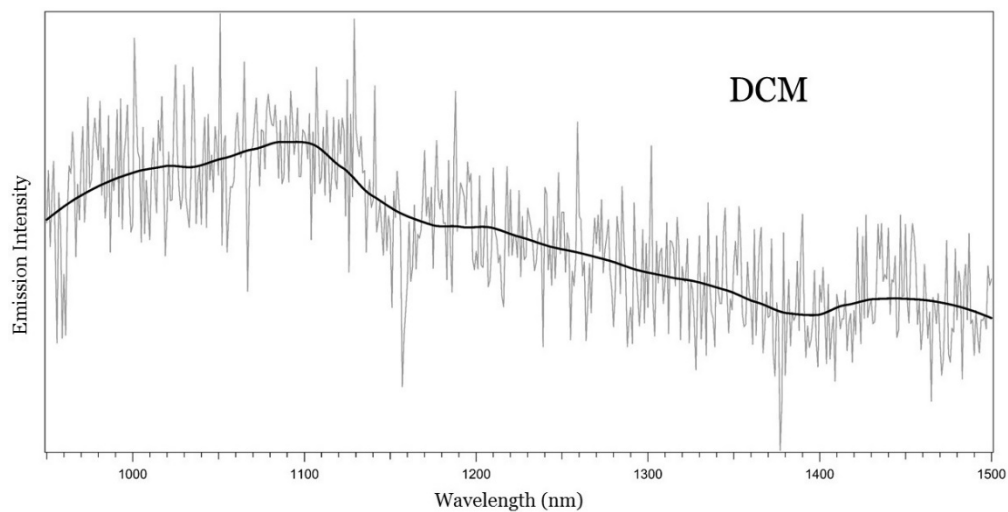
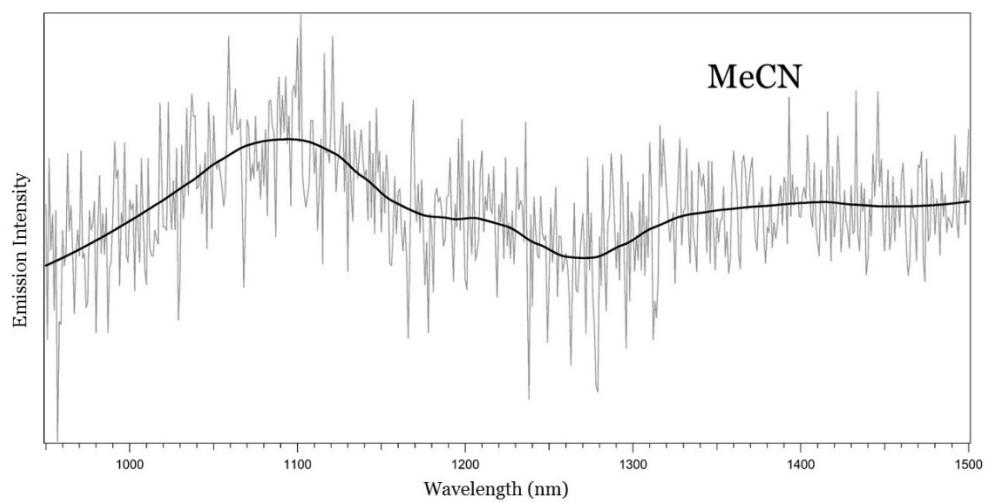


Figure S11. Raw emission data in gray of nanoencapsulated ^{10l}RosIndz in water. Second order LOESS fitted emission data in black with a smoothing constant of 0.3 applied.

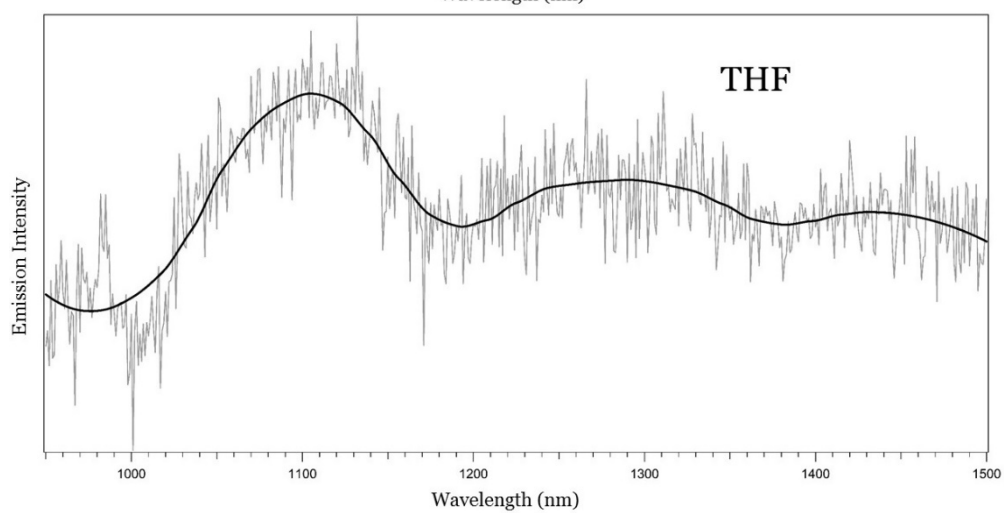
a)



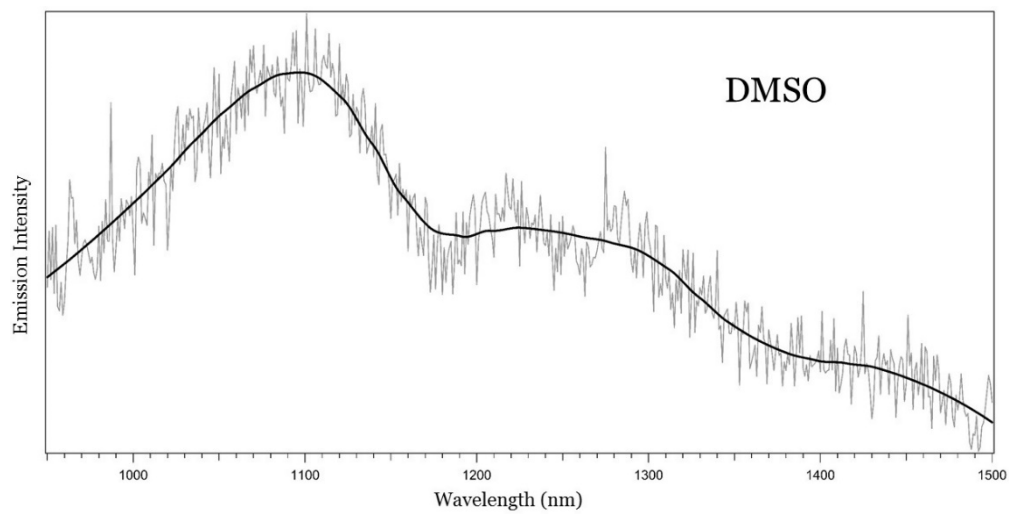
b)



c)



d)



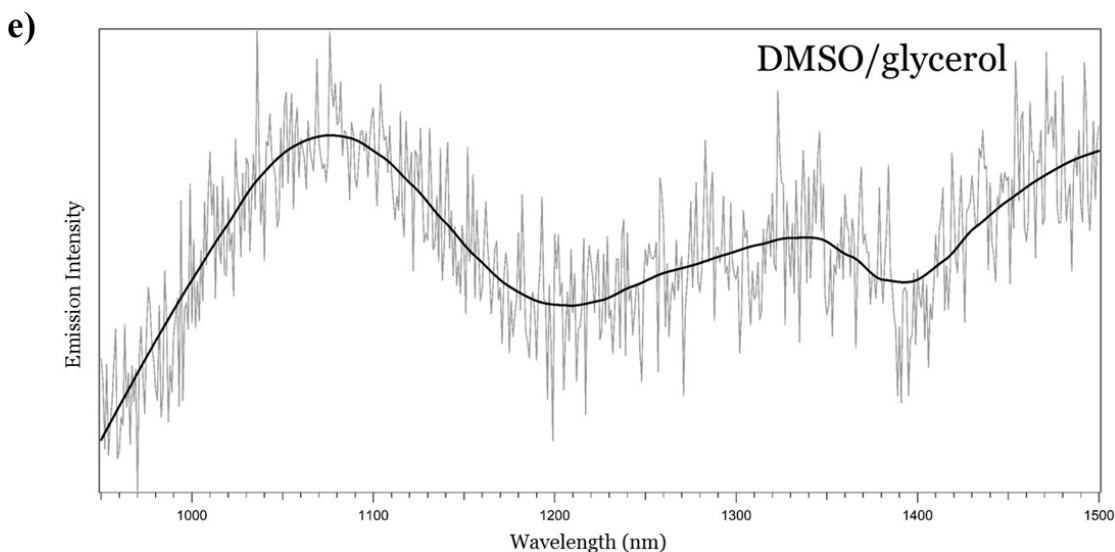


Figure S12. Raw emission data in gray of ^{tol}RosIndz in a) DCM b) MeCN c) THF d) DMSO and e) DMSO/glycerol (25 μ M). Second order LOESS fitted emission data in black with a smoothing constant of 0.3 applied.

Equipment and Experiment Details (TAS)

Excited-state lifetime measurements were conducted using a Helios Transient Absorption Spectrometer (Ultrafast Instruments). Sub-100 fs bandwidth excitation pulses of 950 nm laser light was generated by pumping a Light Conversion optical parametric oscillator (OPO) with the 800 nm fundamental output of a Coherent Astrella fs amplifier. Broadband visible and NIR probe pulses were generated by focusing the 800 nm pulses into calcium fluoride and YAG crystals, respectively. The probe beam was then overlapped spatially with the pump beam to acquire the absorption spectra of the transient species over time. The temporal delay between the pump and probe pulses was controlled using a mechanical optical delay line with a resolution of down to 0.02ps.

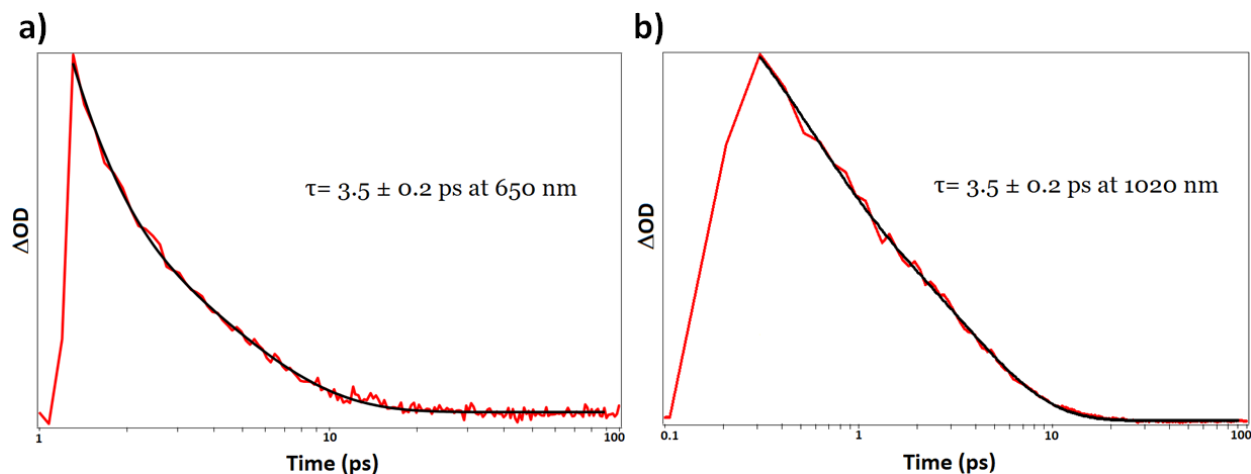


Figure S13. Transient absorption decay plots of encapsulated ^{10l}RosIndz, fitted with the bi-exponential equation, E1 (a) Transient absorption signal (b) Ground state bleaching.

$$y = y_0 + A_1 \exp\left(\frac{-(x-x_0)}{\tau_1}\right) + A_2 \exp\left(\frac{-(x-x_0)}{\tau_2}\right) \quad (\text{E1})$$

The encapsulated ^{10l}RosIndz sample was studied at a concentration of 3×10^{-4} M and the transient absorption lifetime for both the transient absorption increase 650 nm and the ground state bleach at 1020 nm was found to be the same at 3.5 ± 0.2 ps as fit with a double exponential decay (Fig. S13) having a short component of 36% ($A_1 = 0.0111$) and a long component of 64% ($A_2 = 0.0198$).

The free ^{10l}RosIndz sample was studied using the same experimental setup, however the excited state lifetime of the free molecule was shorter than the IRF. The TAS data was collected in both the visible and NIR region.

6. Computational Data

General Information

All the molecules were first drawn in ChemDraw (20.0.0.41) and saved as MDL Molfile. The geometries of those molecules were then optimized with the MMFF94 force field using Avogadro (1.2.0). Dihedral angles of acyclic single bonds were manually set between 0 and 90 degrees to avoid local minima conformations. Then, sequential geometry optimizations were performed by DFT using Gaussian 16³ with the B3LYP^{4,5} functional and the following basis sets: first 3-21G, then 6-31G(d,p),^{6, 7} and finally 6-311G(d,p)⁸ with a dichloromethane polarizable continuum model.⁹⁻¹¹ After having the optimized geometries, TD-DFT were performed with the B3LYP functional and 6-311G(d,p) basis set to compute the vertical transition energies and oscillator strengths.

^{Ph}RosIndz Geometry and Frequency Data

Total Energy of ^{Ph}RosIndz: -2073.368140 Hartrees

Zero imaginary frequencies were found from the optimized geometry of ^{Ph}RosIndz.

XYZ Coordinates of ^{Ph}RosIndz

C	-1.28054	1.71515	0.47947
C	-1.39285	0.36521	0.04446
O	-0.28601	-0.40668	-0.116
C	0.95394	0.08635	0.1293
C	1.13207	1.42778	0.56882
C	-0.00016	2.25257	0.75282
C	-2.49787	2.44697	0.57288
C	-3.70184	1.87242	0.26532
C	-3.79582	0.51331	-0.16593
C	-2.60356	-0.22368	-0.26417
C	2.01177	-0.77955	-0.07896
C	3.33323	-0.35608	0.15083
C	3.52803	0.98751	0.60241
C	2.47652	1.83436	0.81285
C	4.47441	-1.21099	-0.05051
C	-5.06299	-0.11143	-0.45774
C	0.1503	3.65776	1.212
C	-0.3386	4.04735	2.4667

C	-0.18984	5.36219	2.89965
C	0.43107	6.30418	2.08088
C	0.91182	5.92533	0.82863
C	0.78108	4.60794	0.39717
N	4.47749	-2.59056	0.1859
C	5.73934	-3.10371	-0.14617
C	6.54174	-2.04337	-0.60794
C	5.76742	-0.87877	-0.53603
C	3.53259	-3.39525	0.7805
C	3.78059	-4.72345	0.96882
C	5.02112	-5.28687	0.57606
C	5.9905	-4.47679	0.03856
C	-5.49739	-1.4339	-0.18522
C	-6.82903	-1.57182	-0.6008
C	-7.21882	-0.33958	-1.15647
N	-6.13627	0.54763	-1.06411
C	-8.414	0.10054	-1.75774
C	-8.49444	1.36654	-2.28224
C	-7.35629	2.21234	-2.24164
C	-6.20028	1.7902	-1.65355
C	-4.71988	-2.47627	0.52631
C	6.20387	0.45624	-1.00892
C	-4.268	-2.26801	1.83737
C	-3.55927	-3.25971	2.51019
C	-3.28988	-4.47705	1.88507
C	-3.73733	-4.69724	0.58371
C	-4.4485	-3.70572	-0.0898
C	7.31401	1.0885	-0.43173
C	7.73936	2.33457	-0.88811
C	7.06582	2.96564	-1.9325
C	5.9652	2.34231	-2.51973
C	5.53751	1.09877	-2.0625
C	7.94172	-2.19601	-1.12159
C	-7.72763	-2.76285	-0.45441
H	-2.46524	3.47485	0.90641
H	-4.60291	2.45456	0.40117
H	-2.60519	-1.24751	-0.60941
H	1.78422	-1.76157	-0.46851
H	4.53062	1.32527	0.82147
H	2.65917	2.831	1.19021
H	-0.81838	3.31751	3.10828
H	-0.5605	5.64928	3.87662
H	0.53993	7.32851	2.41734
H	1.39103	6.65414	0.18565
H	1.15296	4.31941	-0.57899
H	2.61783	-2.92337	1.09907

H	3.01625	-5.33265	1.43188
H	5.20523	-6.34356	0.72167
H	6.96187	-4.86685	-0.23656
H	-9.2505	-0.58454	-1.80778
H	-9.40848	1.71277	-2.74737
H	-7.38114	3.19706	-2.68833
H	-5.3016	2.38518	-1.64141
H	-4.48339	-1.32808	2.33251
H	-3.22246	-3.084	3.52566
H	-2.73913	-5.24915	2.41006
H	-3.53373	-5.64105	0.09063
H	-4.78765	-3.87979	-1.10468
H	7.83668	0.60633	0.38653
H	8.59645	2.81166	-0.42655
H	7.39781	3.93404	-2.2888
H	5.44159	2.82246	-3.33869
H	4.68777	0.61499	-2.53032
H	8.65952	-2.3384	-0.30651
H	8.25074	-1.31225	-1.6804
H	8.02886	-3.06092	-1.78495
H	-7.29869	-3.49327	0.23206
H	-7.89194	-3.26736	-1.4127
H	-8.70909	-2.47427	-0.06785

^{tol}RosIndz Geometry and Frequency Data

Total Energy of ^{tol}RosIndz: -2112.6946907 Hartrees

Zero imaginary frequencies were found from the optimized geometry of ^{tol}RosIndz.

XYZ Coordinates of ^{tol}RosIndz

C	-1.20572	1.18327	-0.22787
C	-1.17299	-0.23826	-0.19633
O	0.0003	-0.90154	-0.02719
C	1.17402	-0.22896	0.09583
C	1.20681	1.19128	0.03513
C	0.00022	1.90628	-0.11592
C	-2.49048	1.78319	-0.36512
C	-3.62329	1.02475	-0.46351
C	-3.5732	-0.40513	-0.45074
C	-2.31212	-1.01327	-0.30763
C	2.31335	-0.99526	0.25604
C	3.57433	-0.37937	0.36067

C	3.62454	1.04832	0.27827
C	2.49175	1.79856	0.12931
C	4.79354	-1.12711	0.53112
C	-4.7928	-1.16225	-0.56807
C	0.00063	3.39788	-0.17087
C	-0.02171	4.16601	1.01003
C	-0.01796	5.55916	0.88532
C	0.00927	6.18081	-0.36063
C	0.02988	5.41165	-1.52067
C	0.02315	4.0231	-1.42267
C	-0.05371	3.52092	2.37513
N	4.89128	-2.31441	1.26614
C	6.21117	-2.78255	1.19585
C	6.95573	-1.89213	0.39977
C	6.08646	-0.86843	0.00276
C	3.97436	-2.9366	2.08261
C	4.31583	-4.06861	2.76301
C	5.62355	-4.60629	2.65619
C	6.55966	-3.95684	1.89028
C	-6.08374	-0.8699	-0.05281
C	-6.9537	-1.91821	-0.37797
C	-6.21149	-2.85878	-1.11644
N	-4.89238	-2.39529	-1.22272
C	-6.56095	-4.07679	-1.73053
C	-5.62703	-4.77404	-2.456
C	-4.32063	-4.24277	-2.6041
C	-3.97807	-3.0681	-2.00096
C	-6.44129	0.29166	0.79529
C	6.44651	0.23523	-0.91864
C	-7.4555	1.17551	0.401
C	-7.80867	2.25686	1.20586
C	-7.15812	2.46859	2.42018
C	-6.15321	1.59113	2.82639
C	-5.79754	0.51212	2.02163
C	7.4539	1.14824	-0.57679
C	7.80907	2.17461	-1.44988
C	7.16726	2.30126	-2.6806
C	6.16911	1.39398	-3.03455
C	5.81153	0.36981	-2.16182
C	8.39611	-2.08176	0.03026
C	-8.39282	-2.08268	0.00818
H	-2.55674	2.86229	-0.40627
H	-4.57854	1.51353	-0.58942
H	-2.20131	-2.08483	-0.22094
H	2.20248	-2.07009	0.23771
H	4.57991	1.54437	0.36992

H	2.55874	2.87795	0.09311
H	-0.0385	6.16453	1.78507
H	0.01233	7.2629	-0.42318
H	0.04994	5.8846	-2.49532
H	0.03855	3.41627	-2.32093
H	0.85479	2.94243	2.56768
H	-0.89993	2.83555	2.47678
H	-0.13885	4.27688	3.15642
H	3.00258	-2.47865	2.16644
H	3.57199	-4.5395	3.3913
H	5.88238	-5.50947	3.19372
H	7.57702	-4.31869	1.81677
H	-7.5774	-4.43433	-1.62894
H	-5.88674	-5.71104	-2.93165
H	-3.57903	-4.75274	-3.20386
H	-3.00771	-2.61483	-2.11927
H	-7.95922	1.02052	-0.54632
H	-8.5915	2.93369	0.88285
H	-7.43403	3.3088	3.04696
H	-5.64868	1.74397	3.77372
H	-5.02292	-0.17219	2.34823
H	7.95054	1.05988	0.38279
H	8.58651	2.87526	-1.16714
H	7.44459	3.09875	-3.36035
H	5.67119	1.48063	-3.99368
H	5.04211	-0.33834	-2.44734
H	9.06299	-1.85792	0.86982
H	8.67656	-1.4273	-0.79537
H	8.59486	-3.11274	-0.2756
H	-8.66231	-1.39616	0.81126
H	-8.59709	-3.10012	0.3528
H	-9.06431	-1.88427	-0.83414

Table S4. TD-DFT data for the 10 lowest energy vertical transitions with ^{tol}RosIndz.

transition	orbitals	contribution (%)	vertical transition (nm eV)	oscillator strength
S ₀ -> S ₁	H -> L	100	806 1.54	1.023
S ₀ -> S ₂	H-1 -> L	98	654 1.90	0.173
S ₀ -> S ₃	H-2 -> L	99	510 2.43	0.201
S ₀ -> S ₄	H-3 -> L	97	482 2.57	0.012
S ₀ -> S ₅	H-4 -> L H-8 -> L	96 3	438 2.83	0.001
S ₀ -> S ₆	H -> L+1 H-5 -> L H-7 -> L	2 79 15	417 2.97	0.016
S ₀ -> S ₇	H -> L+1 H-4 -> L H-5 -> L H-7 -> L H-8 -> L	3 4 3 4 84	407 3.05	0.004
S ₀ -> S ₈	H-6 -> L	99	398 3.11	0.007
S ₀ -> S ₉	H -> L+1 H-5 -> L H-7 -> L H-8 -> L	4 16 74 5	393 3.16	0.005
S ₀ -> S ₁₀	H -> L+1 H-7 -> L H-8 -> L	86 5 4	391 3.17	0.328

H = HOMO; L = LUMO; S = state

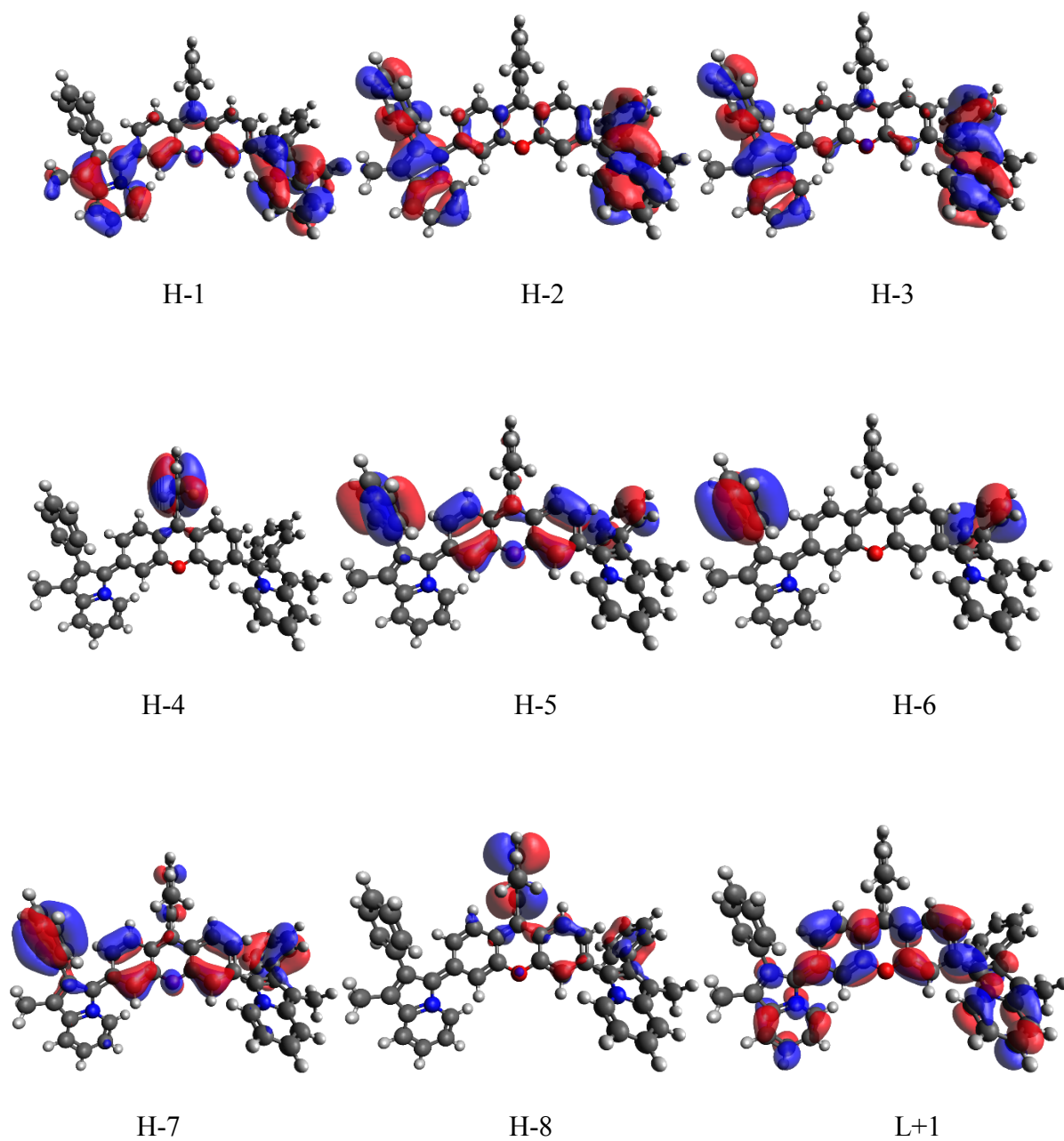


Figure S14. Additional orbital images corresponding to Table S3.

7. Nanoparticle Encapsulation

Formulation of Dye Encapsulated Nanoparticles

^{tol}RosIndz (0.5 mg) and block copolymer (10-PhPCL-G3) (2 mg) were dissolved in a mixture of ACN, THF, and acetone (100 μ L, 50 μ L, and 50 μ L) and added dropwise to MilliQ water (2 mL, 1% TFA) while stirring and sonicating. Organic solvents were removed by allowing them to evaporate under a fume hood. Formulations were allowed to equilibrate for 12 h in the dark, and the unloaded dye was filtered out using a syringe filter (0.45 micron).

Results and Discussion

Because of the promising properties of these dyes as deep-tissue biological imaging agents, understanding the behavior of the dye in an aqueous medium is a vital aspect. In addition to favorable optical properties, aqueous solubility and biocompatibility are crucial for the dye to perform as an efficient imaging agent in biological systems. As ^{tol}RosIndz is hydrophobic, it was initially insoluble in water (Fig. **S15a**). In order to increase the water solubility and biocompatibility, the dye was encapsulated in a biocompatible polymeric nanocarrier system. These nanocarriers are formed by the aggregation of linear dendritic block copolymers (LDBC), 10-PhPCL-G3 (Fig. **S16**), which are made of well-known biocompatible polymeric materials (polycaprolactone (PCL) and polyamidoamine (PAMAM)). These polymeric nanocarriers have shown higher loading efficiencies and better mechanical properties than conventional surfactant-based micelles. The biomimetic nature (i.e., liposome-like morphology) of the nanocarrier has been proven to enhance the systemic circulation time and slow down reticuloendothelial system cleansing. Additionally, LDBC-based nanocarriers have been shown to increase the solubility of NIR imaging agents and delivery into living cells with no noticeable cytotoxicity.¹²

^{tol}RosIndz exhibited a dramatic increase in solubility upon encapsulation in LDBC nanocarriers (Fig. **S15b**). The calculated loading efficiency (DL%) was 15.92 %, which is an excellent loading compared to indolizine based C3 dyes (Table **S5**).¹² According to the LDBC composition and the morphology of the nanoparticle (Fig. **S16**), the dye should be located in the hydrophobic bilayer of the nanoparticle. The intensity average particle size distribution shows a

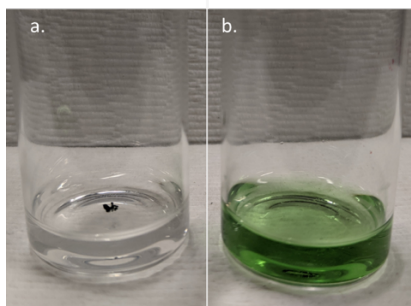


Figure S15. (a) ^{tol}RosIndz in water (b) ^{tol}RosIndz in water after the encapsulation in 10-PhPCL-G3 LDBC nanoparticles.

Table S5. Calculate DL% values for selected indolizine based C3 dyes.

C3	^{tol} RosIndz
2.40	15.92

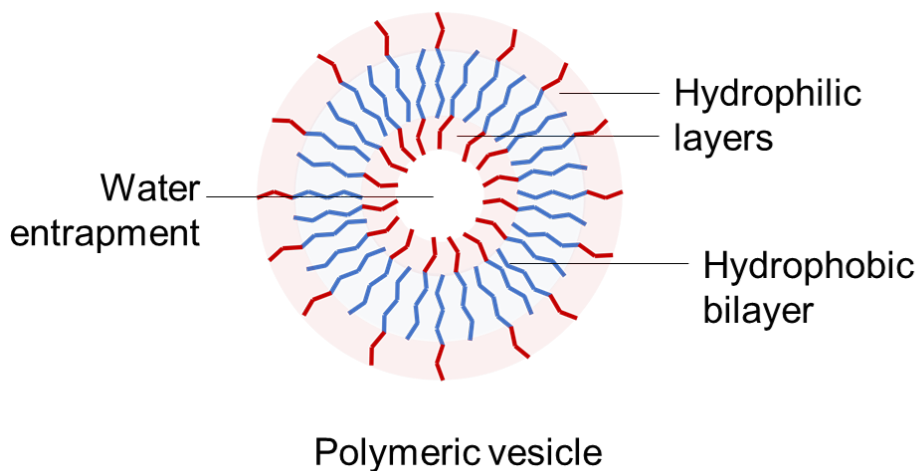


Figure S16. The expected morphology of LDBC nanoparticles based on 70% hydrophobic (blue): 30% hydrophilic (red) polymer-dendron composition.

monodispersed nanoparticle solution with a dispersity of 0.210 and average particle size distribution of 84.18 nm (Fig. S17). The average surface charge of these nanoparticles was 26.8 mV.

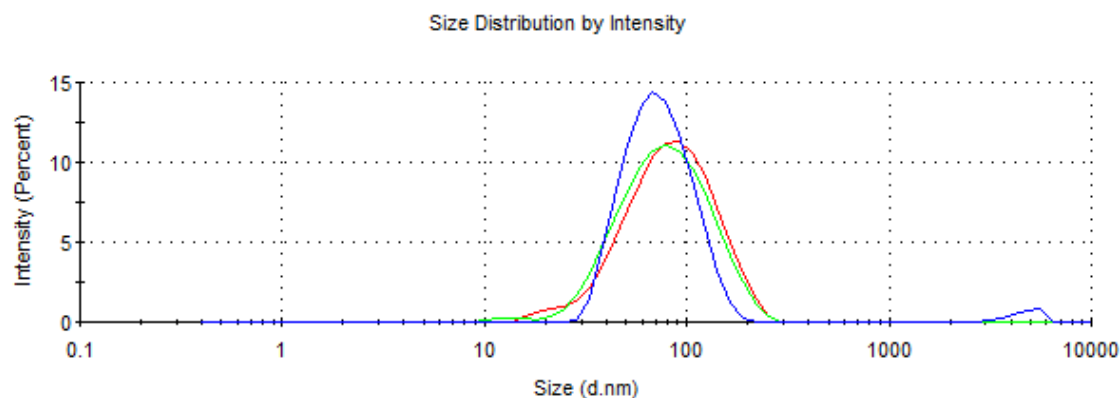


Figure S17. Intensity average size distribution of the ^{tol}RosIndz loaded nanoparticles.

^{tol}RosIndz encapsulated aqueous solutions showed a low energy absorbance maximum wavelength ($\lambda_{\text{max}}^{\text{abs}}$) at 921 nm (Fig. 2). While comparing with the absorption profile of ^{tol}RosIndz in toluene, the encapsulated state does not show significant changes in the peak positions. However, the higher energy vibronic shoulder is more visible in the encapsulated state, presumably due to the aggregated nature of the dye inside the nanoparticle.

8. Cell Toxicity and Uptake

Cytotoxicity Assays

HEK (human embryonic kidney) cells were maintained in standard conditions: DMEM media, 10% FBS, supplemented with penicillin/streptomycin. Cells grown to 70% confluency in 96 well plates were exposed to dendrimer nanoparticles loaded with ^{tol}RosIndz dye or to unloaded nanoparticles. Following a 24-hour incubation, cell media was assessed for the presence of the LDH enzyme released by lysed/damaged cells with the Invitrogen CyQuant LDH Cytotoxicity Assay kit. Colorimetric changes were quantified with a H1 synergy plate reader. Following normalization, percent cytotoxicity was analyzed by ANOVA and Tukey HSD statistical test using a $p \leq 0.5$ threshold through the R language Rmisc and multcomp packages.

Nano-encapsulated ^{tol}RosIndz was then trafficked into human embryonic kidney (HEK) cells, and the cytotoxicity was evaluated by LDH assay. The nano-encapsulated dye showed ≥ 75 % cell viability at the highest tested concentration (50 $\mu\text{g/mL}$) and $\geq 90\%$ cell viability up to 25 $\mu\text{g/mL}$ (Fig. S18). The cell viability values indicate a general nontoxicity of ^{tol}RosIndz loaded nanoparticles in the living cells.

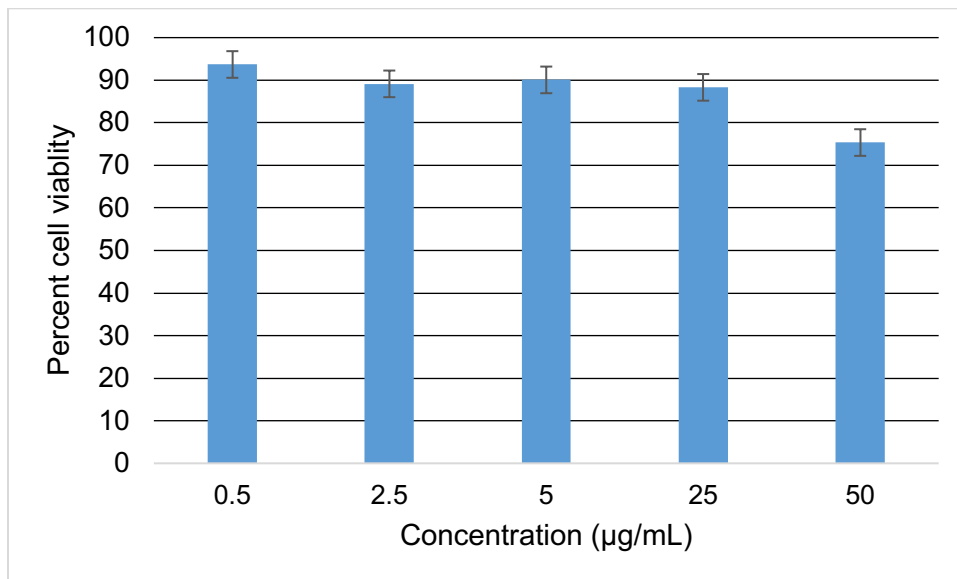


Figure S18. Percent cell viability after encapsulated dye loaded into HEK cells.

9. References

- 1 E. W. Miller, A. E. Albers, A. Pralle, E. Y. Isacoff and C. J. Cheng, *J. Am. Chem. Soc.*, 2005, **127**, 16652-16659.
- 2 A. J. Huckaba, F. Giordano, L. E. McNamara, K. M. Dreux, N. I. Hammer, G. S. Tschumper, S. M. Zakeeruddin, M. Grätzel, M. K. Nazeeruddin and J. H. Delcamp, *Adv. Energy Mater.*, 2015, **5**, 1401629.
- 3 M. J. Frisch, G. W. Trucks, H. B. Schlegel, G. E. Scuseria, M. A. Robb, J. R. Cheeseman, G. Scalmani, V. Barone, G. A. Petersson, H. Nakatsuji, X. Li, M. Caricato, A. V. Marenich, J. Bloino, B. G. Janesko, R. Gomperts, B. Mennucci, H. P. Hratchian, J. V. Ortiz, A. F. Izmaylov, J. L. Sonnenberg, D. Williams-Young, F. Ding, F. Lipparini, F. Egidi, J. Goings, B. Peng, A. Petrone, T. Henderson, D. Ranasinghe, V. G. Zakrzewski, J. Gao, N. Rega, G. Zheng, W. Liang, M. Hada, M. Ehara, K. Toyota, R. Fukuda, J. Hasegawa, M. Ishida, T. Nakajima, Y. Honda, O. Kitao, H. Nakai, T. Vreven, K. Throssell, J. A. Montgomery Jr., J. E. Peralta, F. Ogliaro, M. J. Bearpark, J. J. Heyd, E. N. Brothers, K. N. Kudin, V. N. Staroverov, T. A. Keith, R. Kobayashi, J. Normand, K. Raghavachari, A. P. Rendell, J. C. Burant, S. S. Iyengar, J. Tomasi, M. Cossi, J. M. Millam, M. Klene, C. Adamo, R. Cammi, J. W. Ochterski, R. L. Martin, K. Morokuma, O. Farkas, J. B. Foresman and D. J. Fox, *Gaussian 16, Revision C.01*, 2016, Gaussian, Inc., Wallingford CT.
- 4 A. D. Becke, *J. Chem. Phys.*, 1993, **98**, 5648-5652.
- 5 C. Lee, W. Yang and R. G. Parr, *Phys. Rev. B*, 1988, **37**, 785-789.
- 6 M. M. Francl, W. J. Pietro, W. J. Hehre, J. S. Binkley, M. S. Gordon, D. J. DeFrees and J. A. Pople, *J. Chem. Phys.*, 1982, **77**, 3654-3665.
- 7 W. J. Hehre, R. Ditchfield and J. A. Pople, *J. Chem. Phys.*, 1972, **56**, 2257-2261.
- 8 M. J. Frisch, J. A. Pople and J. S. Binkley, *J. Chem. Phys.*, 1983, **80**, 3265-3269.
- 9 S. Miertus, E. Scrocco and J. Tomasi, *Chem. Phys.*, 1981, **55**, 117-129.
- 10 S. Miertus and J. Tomasi, *Chem. Phys.*, 1982, **65**, 239-245.
- 11 J. L. Pascual-Ahuir, E. Silla and I. Tunon, *J. Comp. Chem.*, 1994, **15**, 1127-1138.
- 12 I. Chandrasiri, D. G. Abebe, M. Loku Yaddehige, J. S. D. Williams, M. F. Zia, A. Dorris, A. Barker, B. L. Simms, A. Parker, B. P. Vinjamuri, N. Le, J. N. Gayton, M. B. Chougule, N. I. Hammer, A. Flynt, J. H. Delcamp and D. L. Watkins, *ACS Appl. Bio Mater.*, 2020, **3**, 5664-5677.